Thermonuclear ^{46}Cr$(p,\gamma)^{47}$Mn rate in type-I x-ray bursts

J. J. He,[1,2,*] A. Parikh,[3,4,†] Y. Xu,[5,6] Y. H. Zhang,[2] X. H. Zhou,[2] and H. S. Xu[2]

[1]*Key Laboratory of Optical Astronomy, National Astronomical Observatories, Chinese Academy of Sciences, Beijing 100012, China*

[2]*Institute of Modern Physics, Chinese Academy of Sciences, Lanzhou 730000, China*

[3]*Departament de Fisica, Universitat Politecnica de Catalunya, Barcelona E-08036, Spain*

[4]*Institut d'Estudis Espacials de Catalunya, Barcelona E-08034, Spain*

[5]*Nuclear Physics Institute, Czech Academy of Sciences, Řež 25068, Czech Republic*

[6]*Extreme Light Infrastructure - Nuclear Physics, 30 Reactorului Street, P.O. Box MG-6, 077125 Magurele, Judeţul Ilfov, Romania*

(Received 28 April 2017; revised manuscript received 23 August 2017; published 2 October 2017)

The thermonuclear rate of the ^{46}Cr$(p,\gamma)^{47}$Mn reaction has been determined using a newly evaluated proton separation energy of $S_p(^{47}\mathrm{Mn}) = 380 \pm 30$ keV and nuclear structure information from the mirror nucleus ^{47}Ti. The astrophysical impact of this new rate and previously available rates has been investigated through one-zone postprocessing type-I x-ray burst calculations. The present ^{46}Cr$(p,\gamma)^{47}$Mn rate leads to a mass fraction at $A = 46$ that is 60 times larger than that obtained using a statistical model rate. The new results constrain the calculated maximum and minimum mass fractions at $A = 46$ and $A = 48$ to be within factors of 12 and 4, respectively. Experimental studies of the level structure of ^{47}Mn near the proton threshold are required to improve these model predictions.

DOI: 10.1103/PhysRevC.96.045801

I. INTRODUCTION

Type-I x-ray bursts (XRBs) arise from thermonuclear runaways within the accreted envelopes of neutron stars in close binary systems [1,2]. About one hundred bursting systems have been identified in the Galaxy, with light curves of about 10–100 s in duration, recurrence periods of approximately hours to days, and peak luminosity $L_{\mathrm{peak}} \approx 10^4$–$10^5\ L_\odot$ (similar, e.g., to L_{peak} of classical novae). During the thermonuclear runaway, an accreted envelope enriched in H and He may be transformed to matter strongly enriched in heavier species (up to $A \approx 100$ [3,4]) via the αp process and the rapid proton capture process (rp process) [5–7]. Current XRB models do not predict the ejection of any appreciable amounts of synthesized material during the burst. Nonetheless, calculations indicate that radiative winds generated during some bursts may eject material [8]. Studies are ongoing to examine the viability of detecting any associated absorption features. For reviews on aspects of type-I x-ray bursts, see, e.g., Refs. [9–11].

The rp process is largely characterized by localized (p,γ)-(γ,p) equilibrium within particular isotonic chains near the proton drip line. Slower β decays [followed by fast (p,γ) reactions] connect these isotonic chains and set the timescale for processing towards heavier nuclei. In such an equilibrium situation the abundance distribution within an isotonic chain depends exponentially on nuclear mass differences as the abundance ratio $Y_{(Z+1,N)}/Y_{(Z,N)}$ between two neighboring isotones is proportional to $\exp[S_p(Z+1,N)/kT]$, where $S_p(Z+1,N)$ is the proton separation energy of nuclide $(Z+1,N)$, and T is the temperature of the stellar environment. In particular, those isotonic chains with sufficiently small S_p values (relative to XRB temperatures: at 1 GK, $kT \approx 100$ keV) need to be known with a precision better than 10–100 keV [6,12,13]. These include, among others, $S_p(^{26}\mathrm{P})$, $S_p(^{43}\mathrm{V})$, $S_p(^{46}\mathrm{Mn})$, $S_p(^{61}\mathrm{Ga})$, $S_p(^{65}\mathrm{As})$, and, of relevance to the present work, $S_p(^{47}\mathrm{Mn})$ [13]. As well, reliable nuclear physics input (including precise mass values and nuclear structure information) is needed for those nuclei along the rp-process path to calculate the thermonuclear reaction rates required for XRB models. Model predictions can then be compared with, e.g., observations of XRB light curves to extract quantitative information about the stellar environments [14].

The earlier thermonuclear ^{46}Cr$(p,\gamma)^{47}$Mn rate calculations relied on those S_p values from the theoretical estimates or on the extrapolations of the mass surface in the earlier atomic mass evaluations. In 2013, the proton separation energy of ^{47}Mn, $S_p = 381 \pm 38$ [15], was experimentally determined for the first time via atomic mass measurement of ^{47}Mn at HIRFL-CSR (Cooler-Storage Ring at the Heavy Ion Research Facility in Lanzhou) [16] in an IMS (isochronous mass spectrometry) mode. Before this work, the Atomic Mass Evaluation (AME) group has evaluated the proton separation energy of ^{47}Mn several times in the past thirty years. The predicted values of $S_p(^{47}\mathrm{Mn})$ were 467 ± 201 keV (AME85 [17]), 78 ± 161 keV (AME93 [18], AME95 [19]), and 75 ± 161 keV (AME03 [20]), respectively. It shows that this experimental value agrees well with the AME85 value, but is much higher than values from the succeeding mass evaluations. Based on this experimental value, the $S_p(^{47}\mathrm{Mn})$ values were reevaluated to be 380 ± 40 keV (AME12 [21]) and 380 ± 30 keV (AME16 [22]), respectively.

Yan *et al.* [15] used a single-zone XRB model to examine the role of uncertainties in S_p of ^{50,51}Co, ^{46,47}Mn, and ^{43}V and found that the impact of this subset of masses on energy generation and the final composition of burst ashes was negligible. This examination was limited, however, by neglecting the dependence of forward (p,γ) rates on the S_p values adopted; only the respective photodisintegration (γ,p)

*hejianjun@nao.cas.cn

†anuj.r.parikh@upc.edu

TABLE I. Parameters for the present ^{46}Cr$(p,\gamma)^{47}$Mn resonant rate calculation. The listed resonances account for the calculated rate below 2 GK. Excitation energies, J^π values, and half-lives for the mirror ^{47}Ti nucleus are adopted from Ref. [32]. Resonance energies were calculated using $E_r = E_x(^{47}\text{Ti}) - S_p$, with $S_p = 380 \pm 30$ keV [22]. Resonance energy uncertainties are estimated to be ± 107 keV, arising from the uncertainty related to mirror level estimation (± 103 keV) and that from the recent AME16 evaluated $S_p(^{47}\text{Mn})$ value (± 30 keV).

$E_x^{47\text{Ti}}$ (keV)	E_r (keV)	J^π	$T_{1/2}$ (ps)	ℓ	C^2S[a]	Γ_p (eV)	Γ_γ (eV)[b]	$\omega\gamma$ (eV)
0.0		$5/2^-$		3	0.002[c]			
159.371(12)		$7/2^-$	210(6)	3	0.547			
1250.7(10)[d]	871	$3/2^-$		1	0.002	1.16×10^{-2}	5.84×10^{-5}[e]	1.16×10^{-4}
1252.09(4)	872	$9/2^-$	0.140(13)	5	0.002	5.69×10^{-8}	4.70×10^{-3}	2.80×10^{-7}
1444.25(4)	1064	$11/2^-$	0.90(14)	5	0.001	4.30×10^{-7}	7.31×10^{-4}	2.58×10^{-6}
1549.65(9)	1170	$3/2^-$	1.5(4)	1	0.548	9.15×10^{1}	4.39×10^{-4}	8.77×10^{-4}
1793.80(16)	1414	$1/2^-$	1.7(17)	1	0.316	3.46×10^{2}	3.87×10^{-4}	3.87×10^{-4}
1825.0(1)	1445	$3/2^+$,$5/2^+$	2.1(19)	2	0.077	1.61×10^{1}	3.13×10^{-4}	7.83×10^{-4}[f]
2163.2(2)	1783	$3/2^-$	0.0251(43)	1	0.027	2.28×10^{2}	2.63×10^{-2}	5.26×10^{-2}
2166.7(2)	1787	5/2	0.019(5)	2;3	0.001	1.48;0.13	3.46×10^{-2}	9.18×10^{-2}[g]
2259.5(2)	1880	$5/2^+$	0.54(12)	2	0.002	4.57	1.22×10^{-3}	3.65×10^{-3}
2297.1(2)	1917	$5/2^-$,$7/2^-$	< 0.01	3	0.007	1.71	9.75×10^{-2}[h]	3.23×10^{-1}[f]
2364.9(2)	1985	$1/2^+$	> 1.53	0	0.037	1.73×10^{3}	4.30×10^{-4}[i]	4.30×10^{-4}
2406.2(2)	2026	$9/2^-$	0.023(7)	5	0.001	8.21×10^{-4}	2.86×10^{-2}	3.99×10^{-3}
2416.3(2)	2036	$1/2^-$ to $7/2^-$	1.0(6)	1;3	0.001	23.5;0.43	6.58×10^{-4}	1.64×10^{-3}[g]
2525.8(2)	2146	$3/2^-$,$5/2^-$	0.094(19)	1;3	0.001	34.6;0.67	7.00×10^{-3}	1.74×10^{-2}[g]
2548.2(2)	2168	$3/2^-$	0.0062(7)	1	0.074	2.76×10^{3}	1.06×10^{-1}	2.12×10^{-1}
2572.9(2)	2193	$1/2^+$	0.53(22)	0	0.032	3.02×10^{3}	1.24×10^{-3}	1.24×10^{-3}
2599.6(2)	2220	$3/2^-$,5/2,7/2	1.3(5)	1;2;3	0.001	44.0;8.72;0.90	5.06×10^{-4}	1.43×10^{-3}[g]
2619.4(2)	2239	$7/2^-$	0.029(8)	3	0.152	1.47×10^{2}	2.27×10^{-2}	9.07×10^{-2}

[a]Averaged values from the (d,p) experiments [36–39], otherwise using an assumed value of 0.001.
[b]Γ_γ values are calculated from the half-life $T_{1/2}$, except as noted.
[c]Present value calculated here by the OXBASH code [40] within a pf model space. An upper limit of 0.03 was set for this state in the (d,t) experiment [44].
[d]Watson *et al.* [43] suggested this state may be a doublet; see text for details.
[e]Γ_γ value is adopted from calculations by Fisker *et al.* [29].
[f]The statistical factor ω is averaged by the two adopted spin values.
[g]Average value based on the different ℓ values listed.
[h]This state has a half-life of < 0.01 ps, and hence $\Gamma_\gamma > 6.85 \times 10^{-2}$ eV. Here, we adopt the calculated value of 9.75×10^{-2} eV by Fisker *et al.* [29].
[i]This state has a half-life of > 1.53 fs, and hence $\Gamma_\gamma < 4.30 \times 10^{-4}$ eV. Even with this maximum Γ_γ value, this resonance contributes negligibly to the reaction rate.

rates were recalculated using detailed balance. The impact of not consistently calculating forward and reverse reactions using the same S_p value has not been well studied in general (but see Parikh *et al.* [13]). In addition, different burst models and assumptions may lead to dramatically different predictions of observable quantities [7,11,23–25]. To explore these issues, we revisit the ^{46}Cr$(p,\gamma)^{47}$Mn rate, estimate its uncertainty, and examine the effects of using different rates (in which forward and reverse rates are calculated with consistent S_p values) in a type-I XRB model.

The level structure of ^{47}Mn is not experimentally known. As such, previous determinations of the ^{46}Cr$(p,\gamma)^{47}$Mn rate have used properties of the mirror nucleus ^{47}Ti [26], statistical model calculations [27,28], and shell model calculations [29]. Hereafter we refer to these previous rates using the nomenclature adopted in the JINA REACLIB database [30]. That is, *laur* refers to the rate of Wormer *et al.* [26], with $S_p(^{47}\text{Mn}) = 470$ keV (AME85 [17]); *rath* refers to the rate of Rauscher and Thielemann [27], with $S_p(^{47}\text{Mn}) = 324$ keV (finite-range droplet macroscopic model FRDM [31]); *ths8* refers to the rate from Ref. [28], with $S_p(^{47}\text{Mn}) = 477$ keV; and *nfis* refers to the revised rate of Fisker *et al.* [29] in REACLIB, with $S_p(^{47}\text{Mn}) = 477$ keV. The latter two calculations used the same S_p value of 477 keV, which is close to that of AME85.

In this work, the thermonuclear rate of the ^{46}Cr$(p,\gamma)^{47}$Mn reaction has been evaluated using the experimental S_p (^{47}Mn) value [22] along with nuclear structure information from the mirror nucleus ^{47}Ti. The astrophysical impact of our new rate and previous rates has been examined through one-zone postprocessing x-ray burst calculations.

II. NEW RATE CALCULATION

A. Resonant rate

We have calculated the resonant component of the ^{46}Cr$(p,\gamma)^{47}$Mn rate using level energies, half-lives and single-particle spectroscopic factors from the mirror nucleus ^{47}Ti [32]. The resonant rate, in units of cm^{3}s^{-1}mol^{-1}, is determined

using the well-known narrow resonance formalism [33–35],

$$N_A\langle\sigma v\rangle_{\rm res} = 1.54\times10^{11}(\mu T_9)^{-3/2} \times\sum_i \omega\gamma_i \exp\left(-\frac{11.605E_r^i}{T_9}\right) {\rm cm^3 s^{-1} mol^{-1}}, \quad (1)$$

where resonant energy E_r^i and strength $\omega\gamma_i$ are in units of MeV for the ith resonance, μ is the reduced mass of the ^{46}Cr + p system in atomic mass units, and T_9 is the temperature in GK. The resonance strength $\omega\gamma$ is defined by

$$\omega\gamma = \frac{2J+1}{2(2J_T+1)}\frac{\Gamma_p\times\Gamma_\gamma}{\Gamma_{\rm tot}}, \quad (2)$$

where $J_T = 0$ is the spin of the ground-state of ^{46}Cr and J is the spin of a ^{46}Cr + p resonance. Γ_p and Γ_γ are the proton and γ-ray partial widths of a resonance, respectively. In the excitation energy range considered in this work, other decay channels are closed [20], so the total width of a level is just $\Gamma_{\rm tot}\approx\Gamma_p+\Gamma_\gamma$.

γ-ray partial widths of the unbound states in ^{47}Mn were estimated using the lifetimes τ of the corresponding bound states in the mirror ^{47}Ti via $\Gamma_\gamma = \hbar/\tau$. Proton partial widths were calculated using the expression

$$\Gamma_p = \frac{3\hbar^2}{\mu R^2}P_\ell(E)C^2S_p \quad (3)$$

where $R = 1.26\times(1+46^{\frac{1}{3}})$ fm is the nuclear channel radius [26], P_ℓ is the Coulomb penetrability factor, and C^2S_p is the proton spectroscopic factor of the resonance. When available, we have adopted spectroscopic factors C^2S_n determined in ^{46}Ti$(d,p)^{47}$Ti measurements [36–39] and assumed $C^2S_p = C^2S_n$ according to charge symmetry.

Parameters for the present ^{46}Cr$(p,\gamma)^{47}$Mn resonant rate calculation over temperatures relevant to XRBs ($T\leqslant 2$ GK) are summarized in Table I. The resonant rate at these temperatures is dominated by contributions from five resonances at $E_r = 871$, 1170, 1783, 1787, and 1917 keV, with the resonance at 871 keV being the single dominant contributor for $T < 1$ GK (see Fig. 1). All of these resonances satisfy the relation $\Gamma_p \gg \Gamma_\gamma$ or $\omega\gamma\approx\omega\Gamma_\gamma$. Note, however, that the levels at $E_r = 871$ and 1917 keV ($E_x = 1251$ and 2297 keV) do not have definite measured half-lives. As such, for these two levels we have adopted the Γ_γ values predicted by Fisker *et al.* [29] for $3/2^-$ and $7/2^-$ levels at $E_x = 1222$ and 2199 keV, respectively. In addition, for the 871-keV resonance, we have determined a value of $C^2S\approx 0.3$ using OXBASH [40] with a pf model space and the $kb3$ [41] and $kb3g$ [42] interactions. This value is significantly larger than the value of $C^2S = 0.002$ from Refs. [32,43]. Given that $\Gamma_\gamma \ll \Gamma_p$ (and hence $\omega\gamma\approx\omega\Gamma_\gamma$) for either choice of C^2S, we have simply adopted the value of 0.002 for this level in Table I. Furthermore, an experimental spectroscopic factor is unavailable for the level at $E_r = 1787$ keV and we have assumed a value of $C^2S = 0.001$. The listed strength of this resonance would not change if $C^2S > 0.001$ (as $\Gamma_\gamma \ll \Gamma_p$); if $C^2S < 0.001$, the total rate would decrease by no more that 23% at 2 GK (see Fig. 1), which is well within our estimated rate uncertainty

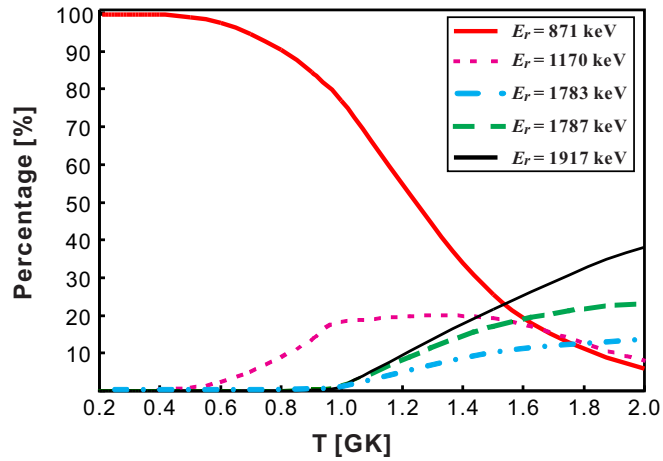

FIG. 1. Percentage contributions of dominant resonances contributing more than 5% to the ^{46}Cr$(p,\gamma)^{47}$Mn resonant rate up to $T = 2$ GK. See text for details.

(a factor of ≈3 at 2 GK, see Table II). Finally, the five resonances at $E_r = 1064$, 2026, 2036, 2146, and 2220 keV also do not have experimental spectroscopic factors, but also do not contribute significantly to the resonant rate for any value of $C^2S_p < 1$. We have simply assumed $C^2S_p = 0.001$ for these levels. It should be noted that four levels in ^{47}Ti [32] (i.e., $E_x = 1670$, 2344, 2499.4, and 2520 keV) were not included in Table I due to the lack of experimental information and their questionable existence.

The uncertainty in the resonant rate was estimated using uncertainties in resonance energies and strengths. The uncertainties in E_r (±107 keV) arise from the experimental $S_p(^{47}$Mn) value (±30 keV [22]) and the uncertainty in the E_x values adopted from the mirror ^{47}Ti, which is assumed to be ±103 keV though a survey of neighboring mirror pairs in the pf-shell region [32,45]. Figure 2 shows energy differences between $T_z = 1/2$ and $T_z = 1$ levels of different mirror pairs, up to excitation energy around 5 MeV. We find the rms energy differences between corresponding levels to be 103 and 87 keV for $T_z = 1/2$ and $T_z = 1$ pairs, respectively. For $T_z = 3/2$, to which the ^{47}Mn–^{47}Ti pair belongs, only two mirror pairs, ^{49}Fe–^{49}V and ^{53}Mn–^{53}Ni, have experimental data, and then for only the first and second excited states. The rms energy difference between corresponding levels for this case is ≈ 30 keV. For $T_z = 2$, only one pair, ^{52}Cr–^{52}Ni, has experimental data, for three excited states. The rms energy difference between corresponding states is ∼ 80 keV. With this information, we assumed a value of ±103 keV for the average energy difference between levels of the ^{47}Mn–^{47}Ti pair. The uncertainties in $\omega\gamma$ are mainly dominated by those of Γ_γ (i.e., the uncertainty in the half-lives listed in Tables I and II) since Γ_γ is usually $\ll\Gamma_p$. An uncertainty of a factor of 2 was assumed for the Γ_γ values adopted from Ref. [29] for the $E_r = 871$ and 1917 keV levels. Uncertainties in Γ_p have been considered through the energy dependence of the penetrability factor P_ℓ [see Eq. (3)].

As shown in Fig. 1, the $E_r = 871$ keV ($E_x = 1251$ keV, $3/2^-$) resonance is a major contributor to the rate up to 1.5 GK.

TABLE II. Rates for the ^{46}Cr$(p,\gamma)^{47}$Mn reaction in units of cm^{3}mol^{-1}s^{-1}.

T_9	Resonant	DC	Total	Lower limit	Upper limit
0.01		2.29×10^{-61}	2.29×10^{-61}	4.57×10^{-62}	1.14×10^{-60}
0.02	2.48×10^{-216}	6.19×10^{-47}	6.19×10^{-47}	1.24×10^{-47}	3.10×10^{-46}
0.03	1.86×10^{-143}	6.19×10^{-40}	6.19×10^{-40}	1.24×10^{-40}	3.10×10^{-39}
0.04	4.48×10^{-107}	1.61×10^{-35}	1.61×10^{-35}	3.21×10^{-36}	8.03×10^{-35}
0.05	2.80×10^{-85}	2.21×10^{-32}	2.21×10^{-32}	4.42×10^{-33}	1.10×10^{-31}
0.06	9.06×10^{-71}	5.46×10^{-30}	5.46×10^{-30}	1.09×10^{-30}	2.73×10^{-29}
0.07	2.02×10^{-60}	4.45×10^{-28}	4.45×10^{-28}	8.90×10^{-29}	2.22×10^{-27}
0.08	1.13×10^{-52}	1.67×10^{-26}	1.67×10^{-26}	3.35×10^{-27}	8.37×10^{-26}
0.09	1.18×10^{-46}	3.59×10^{-25}	3.59×10^{-25}	7.18×10^{-26}	1.80×10^{-24}
0.10	7.58×10^{-42}	5.03×10^{-24}	5.03×10^{-24}	1.01×10^{-24}	2.52×10^{-23}
0.15	1.75×10^{-27}	5.58×10^{-20}	5.58×10^{-20}	1.12×10^{-20}	2.79×10^{-19}
0.20	2.34×10^{-20}	1.97×10^{-17}	1.97×10^{-17}	3.93×10^{-18}	1.22×10^{-16}
0.25	4.10×10^{-16}	1.27×10^{-15}	1.68×10^{-15}	2.55×10^{-16}	1.24×10^{-13}
0.30	2.63×10^{-13}	3.02×10^{-14}	2.93×10^{-13}	8.18×10^{-15}	3.31×10^{-11}
0.35	2.56×10^{-11}	3.79×10^{-13}	2.60×10^{-11}	4.53×10^{-13}	1.78×10^{-09}
0.40	7.76×10^{-10}	3.05×10^{-12}	7.79×10^{-10}	1.84×10^{-11}	3.45×10^{-08}
0.50	8.73×10^{-08}	8.07×10^{-11}	8.74×10^{-08}	3.76×10^{-09}	2.08×10^{-06}
0.60	1.96×10^{-06}	9.77×10^{-10}	1.96×10^{-06}	1.29×10^{-07}	3.07×10^{-05}
0.70	1.78×10^{-05}	7.12×10^{-09}	1.78×10^{-05}	1.60×10^{-06}	2.05×10^{-04}
0.80	9.26×10^{-05}	3.66×10^{-08}	9.26×10^{-05}	1.06×10^{-05}	8.46×10^{-04}
0.90	3.37×10^{-04}	1.46×10^{-07}	3.38×10^{-04}	4.68×10^{-05}	2.55×10^{-03}
1.00	9.72×10^{-04}	4.78×10^{-07}	9.73×10^{-04}	1.59×10^{-04}	6.26×10^{-03}
1.50	4.61×10^{-02}	3.12×10^{-05}	4.61×10^{-02}	1.23×10^{-02}	1.80×10^{-01}
2.00	6.94×10^{-01}	4.29×10^{-04}	6.94×10^{-01}	2.21×10^{-01}	2.21

We have followed the available compilation [32] (see also Watson *et al.* [43]) and assumed a doublet structure around this energy, with one member being $9/2^-$ and the other being either $1/2^-$ or $3/2^-$. For the present calculation we have assumed the lower spin level to be $3/2^-$ given that Fisker *et al.* [29] predicted a $3/2^-$, $E_x = 1221.8$ keV level with the shell model and calculated the associated Γ_γ (see Table I). Note, however, that if this doublet of states is actually only a single $9/2^-$ level, the total resonant rate will be reduced by up to three orders of magnitude, a factor of 4, and 25% at $T < 0.4$, $T = 1.0$, and $T = 1.5$ GK, respectively. Therefore, the nuclear structure of ^{47}Ti around $E_x = 1250$ keV needs to be confirmed through a high-resolution measurement.

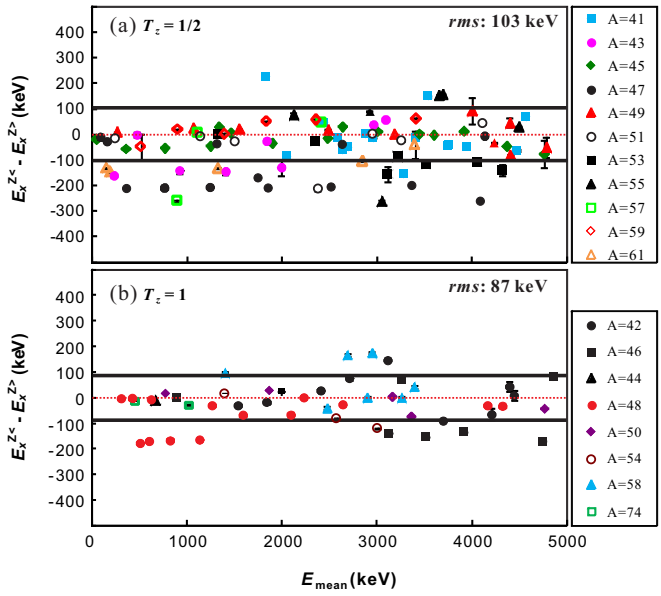

FIG. 2. Energy differences between (a) $T_z = 1/2$ and (b) $T_z = 1$ levels of mirror pairs over $A = 41$–74 [45]. $E_x^{Z<}$ and $E_x^{Z>}$ denote the excitation energies for the members of the pair with lower and higher Z. Here, the rms energy differences are 103 and 87 keV (shown as the solid lines) for $T_z = 1/2$ and 1 pairs, respectively.

B. Direct capture rate

We have estimated the direct capture (DC) component of the ^{46}Cr$(p,\gamma)^{47}$Mn rate using the expression [33,35]

$$N_A\langle\sigma v\rangle_{\rm dc} = 7.83 \times 10^9 \left(\frac{Z_T}{\mu}\right)^{1/3} T_9^{-2/3} S_{\rm dc}(E_0) \times \exp\left[-4.2487\left(\frac{Z_T^2\mu}{T_9}\right)^{1/3}\right] {\rm cm^3 s^{-1} mol^{-1}}, \quad (4)$$

where $Z_T = 24$ is the atomic number of ^{46}Cr. The effective astrophysical S factor at the Gamow energy E_0, $S_{\rm dc}(E_0)$ (in units of MeV b), can be expressed by [35,46],

$$S_{\rm dc}(E_0) = S(0)\left(1 + \frac{5}{12\tau}\right), \quad (5)$$

where $S(0)$ is the S factor at zero energy. The dimensionless parameter τ is given numerically by $\tau = 4.2487(Z_T^2\mu/T_9)^{1/3}$ for proton capture.

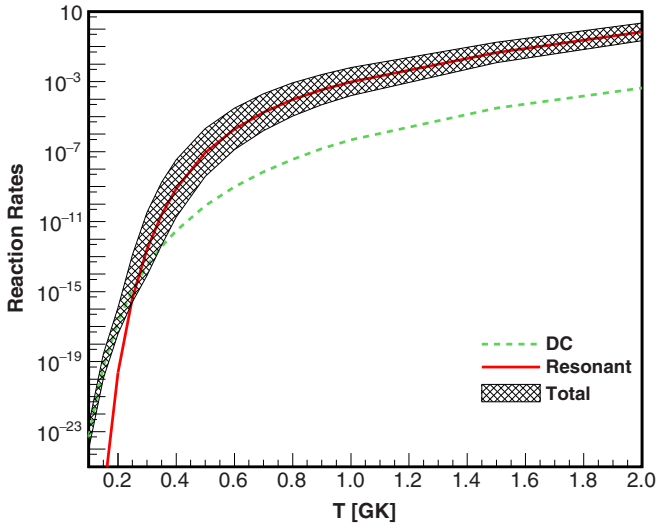

FIG. 3. The presently calculated ^{46}Cr$(p,\gamma)^{47}$Mn reaction rates (in units of cm^{3}mol^{-1}s^{-1}). Here, the grey band indicates the upper and lower limits of the present total rate.

In this work, we have considered direct capture into the ground and first-excited states (predicted at $E_x = 135.5$ keV [29]) of ^{47}Mn. The associated $S(0)$ values were found using the code RADCAP [47,48] based on a Woods-Saxon nuclear potential (central + spin orbit) and a Coulomb potential of a uniform charge distribution, with the nuclear potential parameters determined by matching the bound-state energy. Spectroscopic factors of $C^2S = 0.002$ and 0.547 (see Table I) were adopted for the ground and the first-excited states, respectively. With the parameter set of Huang *et al.* [48] (radius $r_0 = 1.26$ fm, diffuseness $a = 0.65$ fm, $V_{\rm s.o.} = -10$ MeV [33]), we find $S(0) = 3.98 \times 10^4$ and 92.5 eV b for direct capture to the first-excited and ground states of ^{47}Mn, respectively.

The uncertainty of the direct capture component was examined by using different optical-model parameter sets to calculate the $S(0)$ values. Reasonable variations of the radius and diffuseness parameters lead to variations in the DC rate by up to factors of 4% and 30%, respectively. In addition, the uncertainty of $S_p(^{47}\text{Mn})$ contributes an uncertainty of only about 3% to the DC rate. Thus, we adopt an uncertainty of a factor of 5 for the direct capture component of the reaction rate.

Previous estimates of the DC component were made by Wormer *et al.* [26] and Fisker *et al.* [29]. We have reanalyzed the parametrized reaction rate in Ref. [26] together with the JINA REACLIB *laur* rate, and find that Wormer *et al.* adopted a total $S(0) = 3.03 \times 10^4$ eV b, which agrees well with the present results. On the other hand, a value of $S(0) = 3.079 \times 10^2$ eV b was listed in Table I of Ref. [29]. Two issues arise with regard to this value. First, we find that the tabulated DC component of Ref. [29] requires an $S(0)$ value about 30 times larger than their tabulated $S(0)$ value. Second, since Ref. [29] assumed $S_p(^{47}\text{Mn}) = 85$ keV, only direct capture to the ground state could be considered given their prediction of $E_x = 135.5$ keV for the first-excited state; as discussed above, we find that the DC component is dominated by capture to the first-excited state. As such, we do not consider the $S(0)$ value of Ref. [29] further in this work.

C. Total reaction rate

The total thermonuclear proton capture reaction rate is the sum of resonant- and direct-capture components on the ground state and thermally excited states of the target nucleus, weighted with their individual population factors [35]. The probability of populating the ith- excited state (E_i, J_i) of the target nucleus ^{46}Cr can be expressed as

$$P = \frac{(2J_i + 1)e^{-E_i/kT}}{1 + \sum_n (2J_n + 1)e^{-E_n/kT}}, \tag{6}$$

where n is the nth-excited state of ^{46}Cr with corresponding E_n and J_n. The first two excited states in ^{46}Cr are at $E_x = 0.892$ MeV (2^+) and 1.987 MeV (4^+). According to Eq. (6), thermal excitations to these ^{46}Cr levels can be entirely neglected at temperatures relevant to XRBs. This is consistent with stellar enhancement factor (SEF) calculations [27] which find that thermal effects can be neglected below 7 GK.

In this work, the total ^{46}Cr$(p,\gamma)^{47}$Mn reaction rate has been calculated by simply summing the resonant and DC contributions. Here, the DC rate only makes a dominant contribution in the temperature region below ~0.25 GK. The present resonant, DC and total rates are shown in Fig. 3 and summarized in Table II, where the lower and upper limits have been determined using the uncertainties in the resonant and DC components as discussed above.

For $0.01 \leqslant T \leqslant 2$ GK, relevant for XRBs, the present total rate can be parametrized (in units of cm^{3}mol^{-1}s^{-1}) as [27]

$$\begin{aligned} N_A\langle\sigma v\rangle = {} & \exp(814.499 + 3.79T_9^{-1} - 120.966T_9^{-1/3} - 849.986T_9^{1/3} + 171.156T_9 - 25.505T_9^{5/3} + 128.157\ln T_9) \\ & + \exp(9222.44 - 14.508T_9^{-1} + 2400.8T_9^{-1/3} - 14211.1T_9^{1/3} + 3486.06T_9 - 899.31T_9^{5/3} + 3491.56\ln T_9) \\ & + \exp(2337.62 - 3.727T_9^{-1} + 559.548T_9^{-1/3} - 3591.74T_9^{1/3} + 932.636T_9 - 243.78T_9^{5/3} + 860.089\ln T_9). \end{aligned}$$

with fit error less than 2.4%.

Figure 4 shows the present total rate, the associated lower and upper rate limits, and four other ^{46}Cr$(p,\gamma)^{47}$Mn rates compiled in JINA REACLIB (*rath*, *ths8*, *nfis*, *laur*). The present rate uncertainty below 0.25 GK is dominated by the uncertainty of the DC component as discussed above. Between 0.3 and 1 GK, the largest contributor to the rate uncertainty is the assumed ±103 keV uncertainty of the excitation energy for the 871-keV resonance. The statistical-model *rath* and *ths8* rates deviate from the present rate by orders of magnitude for

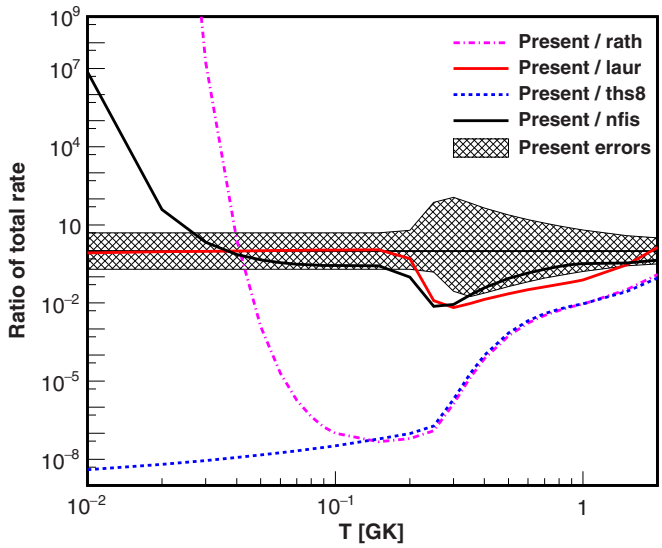

FIG. 4. Ratios between the total ^{46}Cr$(p,\gamma)^{47}$Mn reaction rate from the present work and other rates available in JINA REACLIB [28]. The grey band indicates the upper and lower limits of the present rate.

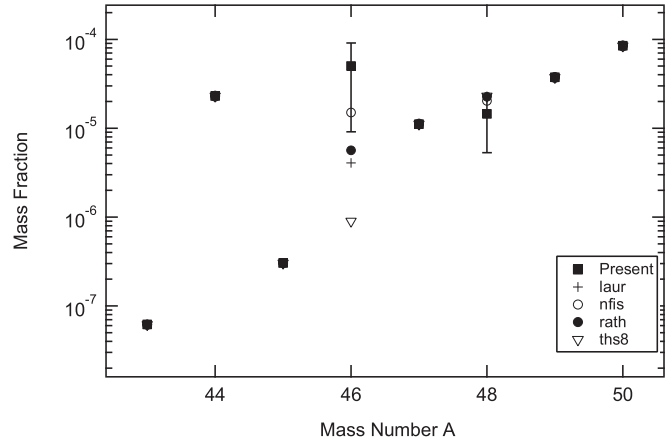

FIG. 5. Selected abundances (as mass fractions summed over mass number) following one-zone XRB calculations with the present and *laur* [26], *nfis* [30], *rath* [27], and *ths8* [30] rates of ^{46}Cr$(p,\gamma)^{47}$Mn. Abundances using lower and upper limits to the present rate (see Table II) are indicated as error bars on the abundances using the present rate. Here, the present ($S_p = 380$ keV) and *laur* ($S_p = 470$ keV) rates are based on information from the mirror nucleus, the *rath* ($S_p = 324$ keV) and *ths8* ($S_p = 477$ keV) rates are based on the statistical model, and the *nfis* ($S_p = 477$ keV) rate is based on the shell model.

$T < 2$ GK (e.g., at 0.01 GK, the present rate is a factor of 10^{51} larger than *rath*, and a factor of 10^8 smaller than *ths8*), but are roughly consistent with the present rate at higher temperatures. This suggests that using the statistical model for this reaction rate at low temperatures is not ideal due to the low density of low-lying excited states in ^{47}Mn. Below 0.03 GK, the present rate is significantly larger than the *nfis* rate. This is likely due to differences in the calculated DC components, as discussed above. For $0.03 < T < 2$ GK, the present and *nfis* rates are in rough agreement, except for the large deviation between 0.2–0.3 GK. The present rate is similar to the *laur* rate below 0.2 GK due to the similar $S(0)$ value and the dominant DC component at lower temperatures. For $0.2 < T < 2$ GK, the present rate is smaller than the *laur* rate because the latter assumed a doublet of states at $E_x = 1.25$ MeV with spins of $3/2^-$ and $1/2^-$, in contrast to the assumption here of $3/2^-$ and $9/2^-$ [32]. However, these two rates are roughly consistent within the present uncertainties.

III. ASTROPHYSICAL IMPLICATIONS

The impact of our new ^{46}Cr$(p,\gamma)^{47}$Mn rate has been examined within the framework of one-zone XRB postprocessing calculations using the K04 ($T_{\rm peak} = 1.4$ GK) model [13,49]. No significant differences (i.e., greater than 5%) in the calculated nuclear energy generation rate were observed when comparing results using the present rate (and the upper and lower limits listed in Table II) and rates determined in previous works (*laur*, *rath*, *nfis*, *ths8*). Nucleosynthesis predictions were also broadly consistent between calculations using these different rates, except at $A = 46$ and 48. As shown in Fig. 5, the abundance at $A = 46$ (shown as a mass fraction, summed over mass number) using the present rate is 60 times larger than that obtained using the *ths8* rate. As well, the abundance at $A = 48$ using the present rate is a factor of ≈ 2 lower than that obtained using the other rates. The uncertainty in the present rate results in yields that differ by factors of 12 and 4 at $A = 46$ and 48 respectively. Uncertainties in the yields determined using the previous rates are not included in Fig. 5 as they are not available. These yield uncertainties would likely be larger than those obtained using the present rate uncertainties simply given the larger uncertainties in the (theoretical) S_p values adopted.

The trends in Fig. 5 can be understood by referring to the relative magnitudes of (a) the different forward (p,γ) rates in Fig. 4 over XRB temperatures (0.2–1.4 GK for the model considered) and (b) the S_p values used with the (p,γ) rates to determine the corresponding reverse photodisintegration (γ,p) rates according to detailed balance. For example, as seen in Fig. 4, the present recommended (p,γ) rate is generally smaller than the *laur* and *nfis* rates over the relevant temperatures. This, in combination with the smaller S_p value used with the present recommended rate (380 keV, as opposed to 470 and 477 keV for the *laur* and *nfis* rates, respectively) leads to more material at $A = 46$ when using the present rate than produced using the *laur* and *nfis* rates, at the end of the burst. The differences between the abundances obtained using the *laur* and *nfis* rates can then be attributed to the differences in the two respective forward (p,γ) rates, as the S_p values are very similar. On the other hand, the *rath* rate uses a smaller S_p value of 324 keV than the present rate, and the *rath* (p,γ) rate is much larger than the present rate over XRB temperatures. These two issues compete as the burst evolves, with the former suggesting more material produced by the *rath* rate than the present rate at $A = 46$, and the latter suggesting less material produced by the *rath* rate than the present rate at $A = 46$. These cases help to illustrate the importance of both the (p,γ) rate and the S_p

value used for the reverse (γ,p) rate in determining the burst ashes.

As shown in Fig. 5, the choice of ^{46}Cr$(p,\gamma)^{47}$Mn rate does not affect the mass fraction at $A = 47$, and the different models predict roughly similar mass fractions at $A = 48$, relative to the differences observed at $A = 46$. This is because the mass fraction at A=47 is not dominated by the contribution from ^{47}Mn, but rather by the contribution from ^{47}Fe, which is not affected by the ^{46}Cr$(p,\gamma)^{47}$Mn rate. Here, the mass fraction of ^{47}Fe is ≈60 times larger than that of ^{47}Mn at the end of the burst, when using the present rate. The mass fraction at $A = 48$ is dominated by the contribution from ^{48}Fe, which is produced through the processes ^{46}Cr$(p,\gamma)^{47}$Mn$(p,\gamma)^{48}$Fe and ^{47}Fe$(\beta^+)^{47}$Mn$(p,\gamma)^{48}$Fe. The amount of ^{48}Fe at the end of the burst arises mostly from the second sequence above due to the large amount of ^{47}Fe that accumulates, β-decays, and is processed via the ^{47}Mn$(p,\gamma)^{48}$Fe reaction.

Differences between our results and those of Yan *et al.* [15] are most likely due to the different XRB models adopted and the more consistent treatment in the present work of using the same S_p value to calculate both forward and reverse rates. Different levels of sophistication in XRB models (postprocessing, one zone, multizone hydrodynamic) can lead to rather different results (see, e.g., Refs. [11,23,50,51]). Moreover, different models using similar approaches can also lead to somewhat different results, even for similar initial conditions [11]. In addition, as shown above, even for reactions with relatively small Q values (relative to the XRB temperatures) that are expected to quickly reach equilibrium between their forward and reverse rates, the precise forward rate can play a role in determining the burst ashes. As such, the dependence of forward (p,γ) rates on Q values should be considered when evaluating the impact of new mass measurements.

Further tests using full multizone hydrodynamic XRB models [7,23–25] are warranted and would help to confirm the role of the ^{46}Cr$(p,\gamma)^{47}$Mn rate on predictions of XRB observables. These models should also be used to define the impact of this reaction on the possible paths of the rp process in this mass region, as these paths depend not only on the initial conditions of the model (see, e.g., Figs. 5 and 6 in Ref. [11]) and the time elapsed, but also on the particular zone considered (see, e.g., Fig. 13 in Ref. [23]).

IV. SUMMARY

With the recent AME16 evaluation value of $S_p(^{47}\text{Mn}) = 380 \pm 30$ keV [22], the thermonuclear rate and associated rate uncertainties of the ^{46}Cr$(p,\gamma)^{47}$Mn reaction have been reevaluated using nuclear structure information from the mirror nucleus ^{47}Ti. Our new rate deviates by many orders of magnitude from previously determined statistical model rates for $T < 1$ GK. This confirms that statistical model calculations are not ideal for this reaction over XRB temperatures, primarily because of the low expected density of low-lying excited states in ^{47}Mn. A high-resolution study of a possible doublet structure in ^{47}Ti around $E_x = 1250$ keV is required to better constrain the rate calculation for XRB models. Of course, a direct study of the level structure of ^{47}Mn below $E_x = 3$ MeV would be preferred. The astrophysical impact of our new ^{46}Cr$(p,\gamma)^{47}$Mn rate has been investigated through one-zone postprocessing type-I x-ray burst calculations. The abundance at $A = 46$ using the present rate is 60 times larger than that obtained using a statistical model rate. The abundance at $A = 48$ using the present rate is a factor of ≈2 lower than that obtained using previous rates. The uncertainty in our new rate gives yields at $A = 46$ and 48 that differ by factors of 12 and 4 respectively. Hydrodynamic XRB model calculations should be performed to further explore the impact of the new rate and its uncertainties.

ACKNOWLEDGMENTS

This work was financially supported by the National Natural Science Foundation of China (Grants No. 11490562, No. 11675229, and No. 11405228) and the National Key Research and Development Program of China (Grant No. 2016YFA0400503). A.P. was partially supported by the Spanish MINECO Grant No. AYA2014-59084-P, by the E.U. FEDER funds, and by the AGAUR/Generalitat de Catalunya Grant No. SGR0038/2014.

[1] S. E. Woosley and R. E. Taam, Nature (London) **263**, 101 (1976).
[2] P. C. Joss, Nature (London) **270**, 310 (1977).
[3] H. Schatz, A. Aprahamian, V. Barnard, L. Bildsten, A. Cumming, M. Ouellette, T. Rauscher, F. K. Thielemann, and M. Wiescher, Phys. Rev. Lett. **86**, 3471 (2001).
[4] V.-V. Elomaa, G. K. Vorobjev, A. Kankainen *et al.*, Phys. Rev. Lett. **102**, 252501 (2009).
[5] R. K. Wallace and S. E. Woosley, Astrophys. J. Suppl. **45**, 389 (1981).
[6] H. Schatz, A. Aprahamian, J. Görres *et al.*, Phys. Rep. **294**, 167 (1998).
[7] S. E. Woosley, A. Heger, A. Cumming *et al.*, Astrophys. J. Suppl. **151**, 75 (2004).
[8] N. N. Weinberg, L. Bildsten, and H. Schatz, Astrophys. J. **639**, 1018 (2006).
[9] W. H. G. Lewin, J. van Paradijs, and R. E. Taam, Space Sci. Rev. **62**, 223 (1993).
[10] T. Strohmayer and L. Bildsten, in *Compact Stellar X-Ray Sources*, edited by W. Lewin and M. van der Klis (Cambridge University Press, Cambridge, 2006).
[11] A. Parikh, J. José, G. Sala, and C. Iliadis, Prog. Part. Nucl. Phys. **69**, 225 (2013).
[12] H. Schatz, Int. J. Mass Spectrom. **251**, 293 (2006).
[13] A. Parikh, J. José, C. Iliadis, F. Moreno, and T. Rauscher, Phys. Rev. C **79**, 045802 (2009).
[14] H. Schatz and K. E. Rehm, Nucl. Phys. A **777**, 601 (2006).
[15] X. L. Yan, H. S. Xu, Yu. A. Litvinov *et al.*, Astrophys. J. Lett. **766**, L8 (2013).
[16] J. W. Xia, W. L. Zhan, B. W. Wei *et al.*, Nucl. Instrum. Methods A **488**, 11 (2002).

[17] G. Audi and A. H. Wapstra, Nucl. Phys. A **432**, 1 (1985).
[18] G. Audi and A. H. Wapstra, Nucl. Phys. A **565**, 1 (1993).
[19] G. Audi and A. H. Wapstra, Nucl. Phys. A **595**, 409 (1995).
[20] G. Audi, A. H. Wapstra, and C. Thibault, Nucl. Phys. A **729**, 337 (2003).
[21] M. Wang, G. Audi, A. H. Wapstra *et al.*, Chin. Phys. C **36**, 1603 (2012).
[22] M. Wang, G. Audi, F. G. Kondev *et al.*, Chin. Phys. C **41**, 030003 (2017).
[23] R. H. Cyburt, A. M. Amthor, A. Heger *et al.*, Astrophys. J. **830**, 55 (2016).
[24] J. L. Fisker, H. Schatz, and F.-K. Thielemann, Astrophys. J. Suppl. **174**, 261 (2008).
[25] J. José, F. Moreno, A. Parikh, and C. Iliadis, Astrophys. J. Suppl. **189**, 204 (2010).
[26] L. Van Wormer, J. Görres, C. Iliadis, M. Wiescher, and F.-K. Thielemann, Astrophys. J. **432**, 326 (1994).
[27] T. Rauscher and F.-K. Thielemann, At. Data Nucl. Data Tables **75**, 1 (2000).
[28] R. H. Cyburt, A. M. Amthor, R. Ferguson *et al.*, Astrophys. J. Suppl. **189**, 240 (2010).
[29] J. L. Fisker, V. Barnard, J. Görres *et al.*, At. Data Nucl. Data Tables **79**, 241 (2001).
[30] JINA Reaclib Database, https://groups.nscl.msu.edu/jina/reaclib/db/.
[31] P. Möller, J. R. Nix, W. D. Myers, and W. J. Swiatecki, At. Data Nucl. Data Tables **59**, 185 (1995).
[32] T. W. Burrows, Nucl. Data Sheets **108**, 923 (2007).
[33] J. J. He, A. Parikh, B. A. Brown, T. Rauscher, S. Q. Hou, Y. H. Zhang, X. H. Zhou, and H. S. Xu, Phys. Rev. C **89**, 035802 (2014).
[34] Y. H. Lam, J. J. He, A. Parikh *et al.*, Astrophys. J. **818**, 78 (2016).
[35] C. E. Rolfs and W. S. Rodney, *Cauldrons in the Cosmos* (University of Chicago Press, Chicago, 1988).
[36] J. Rapaport, A. Sperduto, and W. W. Buechner, Phys. Rev. **143**, 808 (1966).
[37] J. L. Alty, L. L. Green, G. D. Jones, and J. F. Sharpey-Schafer, Nucl. Phys. A **100**, 191 (1967).
[38] D. C. Kocher and W. Haeberli, Nucl. Phys. A **196**, 225 (1972).
[39] M. S. Chowdhury and H. M. Sen Gupta, Nucl. Phys. A **229**, 484 (1974).
[40] B. A. Brown, E. Etchegoyen, W. D. M. Rae, and N. S. Godwin, OXBASH, 1984 (unpublished).
[41] A. Poves and A. P. Zuker, Phys. Rep. **70**, 235 (1980).
[42] A. Poves, J. Sánchez-Solano, E. Caurier, and F. Nowacki, Nucl. Phys. A **694**, 157 (2001).
[43] D. L. Watson, D. N. Slater, and G. Brown, J. Phys. G **6**, 369 (1980).
[44] H. Pohl, R. Santo, and G. J. Wagner, Z. Phys. **245**, 216 (1971).
[45] Evaluated Nuclear Structure Data File (ENSDF) Retrieval, http://www.nndc.bnl.gov/ensdf/.
[46] W. A. Fowler, G. R. Caughlan, and B. A. Zimmerman, Annu. Rev. Astron. Astrophys. **5**, 525 (1967).
[47] C. A. Bertulani, Comput. Phys. Commun. **156**, 123 (2003).
[48] J. T. Huang, C. A. Bertulani, and V. Guimarães, At. Data Nucl. Data Tables **96**, 824 (2010).
[49] A. Parikh, J. José, F. Moreno, and C. Iliadis, Astrophys. J. Suppl. **178**, 110 (2008).
[50] A. Parikh, J. José, and G. Sala, AIP Adv. **4**, 041002 (2014).
[51] H. Schatz and W.-J. Ong, Astrophys. J. **844**, 139 (2017).